Cytometry
PART A
Journal of the International Society for Advancement of Cytometry

Constrained Watershed Method to Infer Morphology of Mammalian Cells in Microscopic Images

Nezamoddin N. Kachouie,[1,2,3] Paul Fieguth,[3]* Darik Gamble,[4,5] Eric Jervis,[4] Zoheir Ezziane,[6,7] Ali Khademhosseini[1,2]

[1]Department of Medicine, Center for Biomedical Engineering, Brigham and Women's Hospital Harvard Medical School, Boston, Massachusetts

[2]Harvard-MIT Division of Health Sciences and Technology, Massachusetts Institute of Technology, Cambridge, Massachusetts

[3]Department of Systems Design Engineering, University of Waterloo, Waterloo, Canada

[4]Department of Chemical Engineering, University of Waterloo, Waterloo, Canada

[5]Department of Biomedical Engineering, Johns Hopkins University, Baltimore, Maryland

[6]Department of Genetics, Harvard Medical School, Boston, Massachusetts

[7]Department of Information Technology, Women's College, Higher Colleges of Technology, Al Ain, United Arab Emirates

Received 12 January 2010; Revision Received 22 June 2010; Accepted 23 June 2010

*Correspondence to: Paul Fieguth, Department of Systems Design Engineering, University of Waterloo, Waterloo, Canada

Email: pfieguth@uwaterloo.ca (image processing) and ericjj@cape.uwaterloo.ca (cell experiments)

Published online 24 September 2010 in Wiley Online Library (wileyonlinelibrary.com)

DOI: 10.1002/cyto.a.20951

ISAC
International Society for Advancement of Cytometry

Abstract

Precise information about the size, shape, temporal dynamics, and spatial distribution of cells is beneficial for the understanding of cell behavior and may play a key role in drug development, regenerative medicine, and disease research. The traditional method of manual observation and measurement of cells from microscopic images is tedious, expensive, and time consuming. Thus, automated methods are in high demand, especially given the increasing quantity of cell data being collected. In this article, an automated method to measure cell morphology from microscopic images is proposed to outline the boundaries of individual hematopoietic stem cells (HSCs). The proposed method outlines the cell regions using a constrained watershed method which is derived as an inverse problem. The experimental results generated by applying the proposed method to different HSC image sequences showed robust performance to detect and segment individual and dividing cells. The performance of the proposed method for individual cell segmentation for single frame high-resolution images was more than 97%, and decreased slightly to 90% for low-resolution multiframe stitched images. © 2010 International Society for Advancement of Cytometry

Key terms

microscopic image sequence; hematopoietic stem cell; cell uropodia; automated cell shape analysis; watershed segmentation; inverse problem; biomedical image analysis

ADVANCED techniques in digital image processing and pattern recognition can potentially be applied to a large number of digital cytometry systems to improve our understanding of cellular and intercellular events and to direct new discoveries in biological and medical research.

Hematopoietic stem cells (HSCs) form blood and immune cells and are responsible for the constant renewal of blood. To produce new blood cells, HSCs proliferate and differentiate to different blood cell types (1). To analyze stem-cell behavior and infer cell features, the localization, segmentation, and tracking of HSCs in culture is crucial. In our previous work we addressed cell detection/localization (2,3) and the association of detected cells (4). Yet to infer the cell features, we need to outline the boundaries of individual, touching, and dividing cells.

Previously, in vitro time-lapse video microscopy has been used to identify phenotypic traits associated with in vivo HSC functionality. Specifically, longer cell-cycle times were correlated with the retention of HSC activity, and the presence of lagging posterior projections (uropodia) was correlated with the loss of HSC activity (5).

Various time-lapse studies were conducted on HSCs to provide information on their morphology, migration, and localization. For example, individual immature hematopoietic cells were examined to determine the differences in migration mechanisms caused by the primitive nature of the cells (6). This helped to explain the loss of phenotypic function during stem cell differentiation. Also a time-lapse video

monitoring experiment was used to track HSCs and to identify specific parameters related to their self-renewal division (7).

To classify HSCs to different groups, they must be observed/tracked over time and their key features, including cell size, shape, and motility, must be extracted (1,8,9). Manual tracking of such data is an onerous task, and yet still widely practiced, so automated methods are in high demand. Cell segmentation in microscopic images as an object segmentation problem remains an attractive and challenging task due to the often corrupted or blurred images, high noise, the presence of clutter, and the difficulties of adapting and extending available image segmentation approaches (10–13).

A variety of semi-automatic or automatic methods have been proposed for cell segmentation. Geusebroek et al. (14) introduced a method based on Nearest Neighbor Graphs to segment the cell clusters. Meas-Yedid et al. (15) proposed a method to quantify the deformation of cells using snakes. Kittler and Illingworth (16), Otsu (17) and Wu et al. (18) have used thresholding methods. The mean shift procedure method was proposed by Comaniciu and Meer (11) for cell image segmentation for diagnostic pathology. Watershed has been used by Markiewicz et al. (19) for segmentation of bone marrow cells.

Conventional segmentation methods perform poorly when they are applied to Differential Interference Contrast (DIC) cell images. We will show, later in this article, that watershed as a conventional segmentation method cannot segment the DIC cell images. To solve this challenge, in this article the cell segmentation problem is formulated as an inverse problem, and a constrained watershed algorithm is proposed to localize individual cells, outline their boundaries, and measure their features. In a typical inverse problem the model parameters are estimated based on the data, where here the cell centroid is the cell model parameter to be estimated. The proposed method has been successfully applied for modeling HSCs and identifying their locations in DIC microscopic images.

Materials

Wild-type factor-dependent cell-Paterson1 cells (FDC-P1, ATCC Number CRL 12103) were maintained in RPMI (Hyclone, Logan) and 10% FBS, 4 mM L-glutamine, 1× penicillin and streptomycin (Invitrogen, Carlsbad).

Cell imaging chambers were custom-made and loaded, as previously described in Ref. (20) and summarized as follows. A small strip (10 × 2 mm) of glass Fisher microscope cover glass (22 × 50 mm) was washed with 10% NaOH and 1% HCl, dipped in methanol, and dried under nitrogen gas. Glass rectangular tubing (15 × 35 mm inner dimensions) was cut to a height of 8 mm and glued to the cover glass, using Dow Corning silicone medical adhesive, to serve as chamber walls. Lids were cut and assembled from Fisher microscope slides to loosely fit over the walls. After drying for 24 hours, chambers and lids were autoclaved. Chambers were then rinsed in PBS, and coated with 5% BSA and 100 μL/mL fibronectin at 4°C overnight. Studies with a variety of primary and cell lines have confirmed that cells in this environment grow normally.

Cell suspension was spun down to approximately 1 million cells/mL, and mixed 10:1 with a solution of PBS containing 10 μm diameter polystyrene beads at a concentration of 1 million beads/mL. Approximately 20 μL of this cell/bead solution was pipetted into the gap chamber. The remaining cell suspension was rinsed from the sides of the gap chamber by PBS, and then 450 mL of PBS was added to fill the remainder of the chamber. The polystyrene beads stop the glass strip from compressing completely to the bottom of the chamber, which then enforces a monolayer of cells in the imaging chamber, allowing for unambiguous cell tracking over the course of hours or days. During imaging, chambers were maintained at 37°C, in a 5% CO_2 humidified air environment.

Cells were imaged on an inverted microscope (Axiovert 200, Zeiss Germany). A custom-designed robotically controlled stage allowed for multiple adjacent fields of view to be captured as a mosaic. The focus was adjusted for each image independently. Images were captured in a 5 × 5 mosaic at 3-minute intervals using a digital camera (XCD-SX910, Sony, Tokyo, Japan) for 6 hours. The focus was adjusted at 2 and 4 hours to account for focal drift.

Methods

In our previous work (2), we characterized a typical cell in a microscopic image as an approximately circular object with a darker interior and a brighter boundary. The proposed cell model works well to localize that specific HSC phenotype; however, the performance of the algorithm drops if there are significant illumination variations during DIC imaging, or for HSC phenotypes that do not maintain a uniformly bright boundary and dark interior.

Although our previous methods (2,21) perform well for locating cells, they are not capable of accurately modeling dividing cells or localizing individual cells in crowded cell locations. As a result they may fail to locate multiple adjacent cells and in turn are prone to generate erroneous results in such cases. In Ref. (3), we showed that locating the cell centers is essentially an inverse problem which can be addressed in the form of a deconvolution problem. To solve the problem, we proposed to find a set of cell shape parameters, solving the inverse problem using an optimized ellipse fitting method, considering each ellipse centroid as a cell center. The proposed method effectively models dividing and crowded cells, and is capable of modeling different cell types with changes in the model parameters; however, by assuming a fixed, parametric shape, the method is unable to segment cells having complex shapes.

In this article we propose a method to outline the cell boundary. As in Ref. (3), we consider cell segmentation as an inverse problem, addressed as a constrained watershed method. However, in contrast to the method presented in Ref. (3), which localized cells by assuming a parameterized shape, in this article we will solve the cell segmentation problem, given previously localized cells.

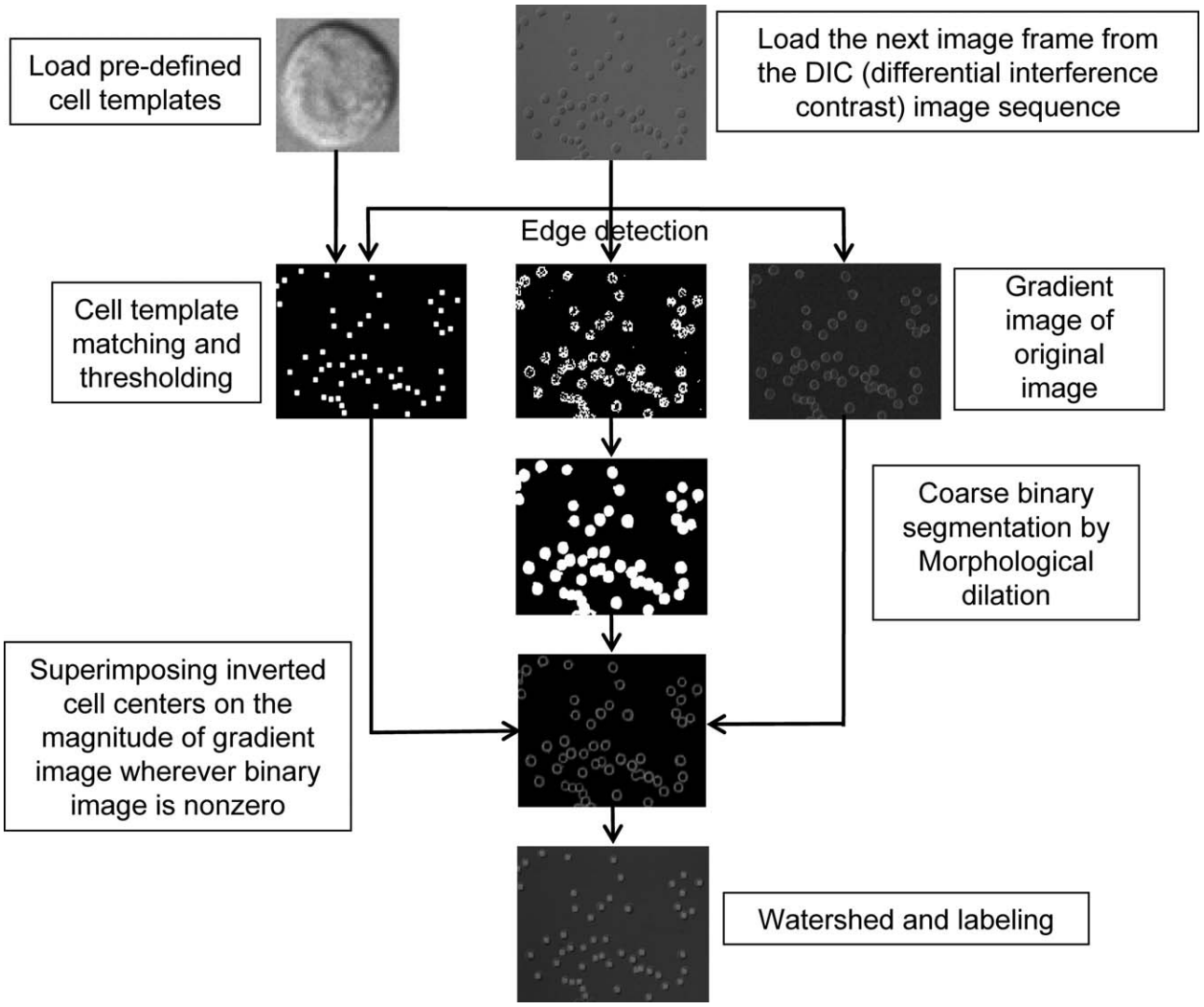

Figure 1. Schematic representation of the proposed method to localize the cells, to detect cell and aggregate boundaries, and to segment individual cells.

The schematic representation of the proposed method is depicted in Figure 1. It has four stages: uneven background correction, coarse segmentation, cell localization, and fine cell segmentation. A preliminary version of watershed segmentation was addressed in Ref. (22), on which we build in this article with a more robust version of constrained watershed with contrast enhancement and correction for the uneven cell boundary illumination caused by DIC imaging. The proposed method can be also applied to down-sampled stitched images with a resolution much lower than that of the original subframes.

Cell Segmentation

As part of an extensive research program to quantify cell phenotypes, the ultimate goal of this project is to classify the presence or lack of cell uropodia. To detect such uropods, it is essential to accurately segment the cell boundaries. Conventional segmentation methods perform poorly when they are applied to DIC cell images due to the short range of gray level intensities, spurious edges, and dividing and crowded cells. Boundary/edge detection methods such as Canny (23) fail to detect the boundary due to spurious edges inside the cell area. Region segmentation methods (24) also fail to segment the cell regions due to over- and under-segmentation. Even combined region-boundary methods (25,26), which combine edge detection and region segmentation, do not solve the problem in their conventional forms due to dividing, touching, and crowded cells.

Our proposed method is a watershed based approach. Watershed, as a typical region boundary approach in its conventional form (25–27), performs very poorly to segment cells in DIC images. Our proposed approach therefore builds on watershed, in which cells are first crudely segmented such that a segment may represent one or more cells. Cell centers are

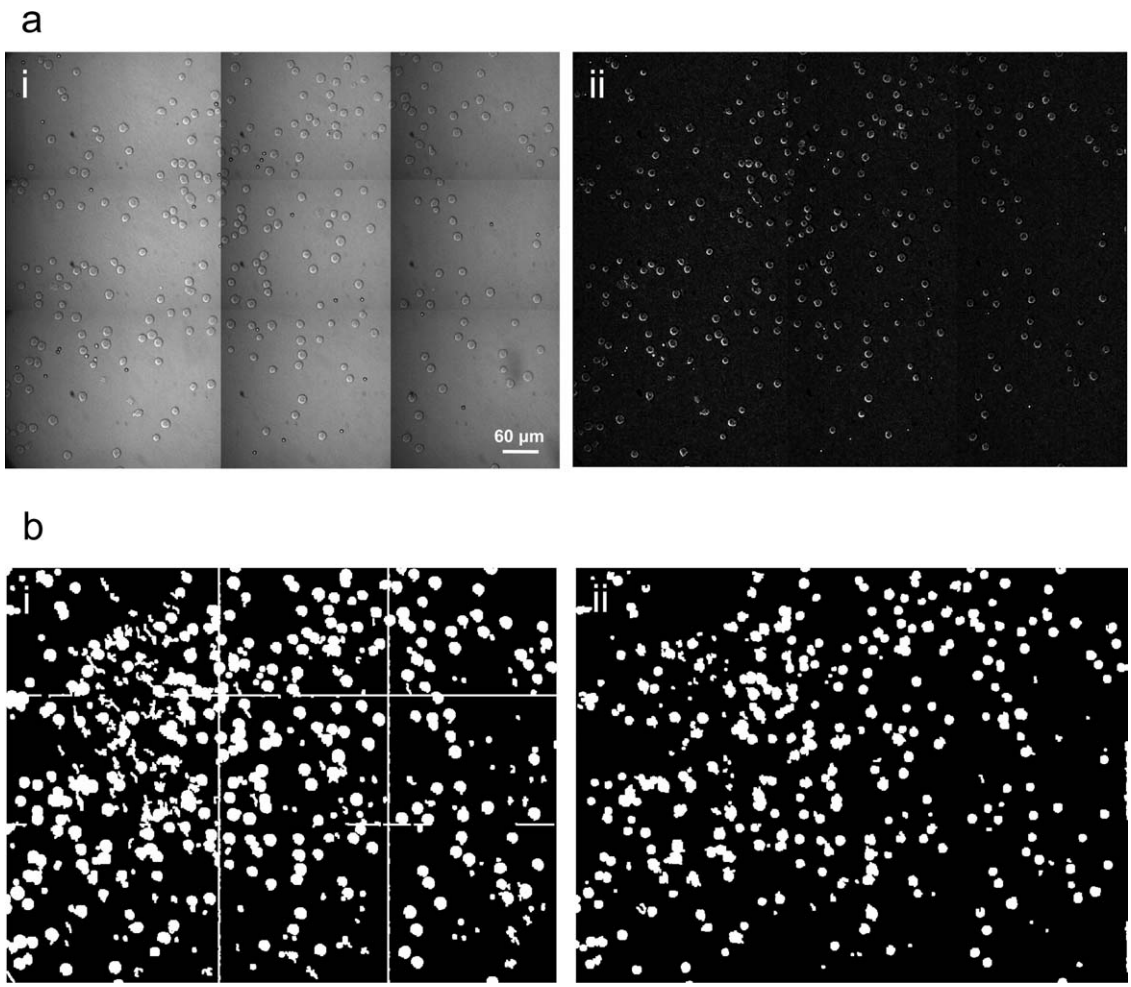

Figure 2. (**a**) A typical stitched image formed by the stitching of nine subframes. i: Original stitched frame with nonuniform background caused by uneven illumination. ii: Corrected image obtained by applying the top hat filtering to (i). (**b**) The application of edge detection followed by morphological dilation. i: To the original stitched image in a (i). ii: To the corrected stitched image in a (ii).

then localized using the original unprocessed image; with the cell centers used as seeds for watershed, a detailed cell segmentation is obtained. Each step is described in greater detail below.

Correction for Uneven Illumination

Let $I = (I_1, I_2, \ldots, I_K)$ be a set of K images, where I_k is the image at time k defined on a fixed discrete grid D:

$$I_k = \{I_{ijk} | (i, j) \in D\} \quad (1)$$

Figure 2a (i) shows a typical stitched 1,280 × 960 image, consisting of nine subframes, each downsampled from their original size. It can be observed that the illumination is uneven over each subimage, therefore a top-hat filter is applied to the image I_k to correct the illumination changes:

$$I_{\text{th}} = I_k - (I_k \, o \, f_s) \quad (2)$$

where I_{th} is the filtered image, f_s is the filter structuring element, and (o) is morphological opening. The filtered image is depicted in Figure 2a (ii) where the uniform background intensity can be very clearly seen.

Edge Detection and Coarse Segmentation

A coarsely segmented image must first be generated before proceeding to the segmentation of finer detail. To achieve this, an edge image is generated by applying Canny edge detector (23), E, to the background corrected image frame I_{th} from Eq. (2):

$$e_k = E(I_{\text{th}}) \quad (3)$$

Cell areas are then coarsely segmented using morphological operators, by dilating a disk M, having a radius of seven pixels, as a morphological mask over the edge map

$$S_k = e_k \oplus M \quad (4)$$

Morphological opening will then be applied to the dilated image to remove those tiny regions considered unlikely to be part of a cell:

$$O_k = S_k \circ O \tag{5}$$

A disk O having a radius of eleven pixels was used for morphological opening in Eq. (5). The image O_k will be later used to preserve portions of the magnitude image for fine segmentation. With the coarse segmentation in place, we next to perform cell localization.

Cell Localization

Cell localization is an essential step in accurate boundary segmentation. Our previously proposed cell detector, in Ref. (2), was based on the attributes of a specific cell phenotype, e.g. bright boundary and dark center. Here we propose a more general approach in which the user may specify or generate a cell template based on data. Let z_k be the set of q_k cell centers in image frame k:

$$z_k = \left\{ z_k^i | i \in [1, q_k] \right\} \tag{6}$$

A cell template is generated from ground-truth cell location data, with the selected cells averaged to generate a cell template

$$h = \frac{1}{N_c} \sum\nolimits_1^{N_c} \mathrm{C_n} \tag{7}$$

averaging over N_c located cells. The cell template h is then convolved with the original image I_k to generate a correlation map:

$$H_k = I_k * h \tag{8}$$

The local maxima identify peaks in the correlation map, therefore to locate the cell-center candidates, we find the local maxima

$$L_k = l(H_k, d_l) \tag{9}$$

where l locates the largest local maxima in the correlation map H_k, with a minimum separation of d_l. Since the noise in the image background will give rise to exceptionally weak maxima, the mostly likely cell centers are generated by thresholding L_k to remove inconsequential maxima:

$$Z_k = T(L_k, \tau) \tag{10}$$

where T is a thresholding function, returning only those local maxima in L_k whose values exceed threshold τ. The threshold τ is set experimentally to minimize the number of misdetections and false alarms.

Constrained Watershed

Empirically we have found conventional watershed to perform very poorly on cell images because of a failure to separate grouped and dividing cells. Our proposed approach is to seed the watershed approach by actually placing dark spots at every detected cell center, forcing the creation of watershed regions. In this way the local minima direct the watershed method to converge toward the cell boundaries.

To outline the cell boundaries, a gradient image of the original image is obtained (G_k), its magnitude M_k is computed, and those portions of the magnitude image corresponding to the coarsely segmented binary image O_k will be preserved by computing the pixel by pixel product of these two images, $P_k = M_k \odot O_k$, considering each pixel in binary image O_k to be either 1 or 0. The detected cell centers (see Cell Localization) are then inverted and superimposed on the preserved magnitude image as local minima.

Let $z_k = \{z_k^i | \ i \in [1, \ q_k]\}$ be the set of cell centers in cell center map Z_k consisting of q_k centers. The set of points $d \in D$ (where D is a digital grid) which are topographically closer to a cell center z_k^i than to any other cell center z_k^j construct the cell region $R(z_k^i)$ which is associated with the cell center z_k^i. The watershed of g is a set of points which do not belong to any cell region and represents the cell boundaries W:

$$W(g) = D \backslash \left(\cup_{i \in [1, q_k]} R\left(z_k^i\right) \right) \tag{11}$$

In this way watershed partitions the superimposed magnitude image by filling the imposed inverted cell centers (local minima). The intent is that watershed catchment basins will represent cell regions, and the watershed segmentation lines demarcate cell boundaries.

Results and Discussion

In this section we present the detection/segmentation results generated by applying the proposed method. The proposed algorithm was developed in Matlab and used for cell segmentation in DIC images, applied to several hundred frames from different data sets. To test the performance, the automated cell segmentation was compared with ground truth obtained from manual cell tracking, carried out by operators trained on a sample data set. Manual tracking and automatic segmentation were considered to match when a manually tracked cell was contained within the bounding box of a segmented cell. In the following tests, a single cell template was used as correlation kernel; however, in future work we plan to allow more flexible templates based on cell type and shape.

A typical multiframe stitched microscopic image is depicted in Figure 2a (i). The background-corrected image using top hat filtering is depicted in Figure 2a (ii), where we can clearly see the uniformity of the background intensity. As is shown in Figure 2a, uneven illumination over the subframes in the stitched image contributes greatly to the detection of spurious edges, as shown in Figure 2b (i). In contrast, as seen in Figure 2b (ii), there are no significant subframe boundaries detected in the corrected image.

As is typical in watershed segmentation, we use the magnitude of the gradient image to partition the image to different segments. However, watershed in its conventional form performs very poorly and segments dividing cells as a single object. To overcome this shortcoming the proposed constrained watershed takes advantage of the detected cell centers to direct watershed towards boundaries of connected cells.

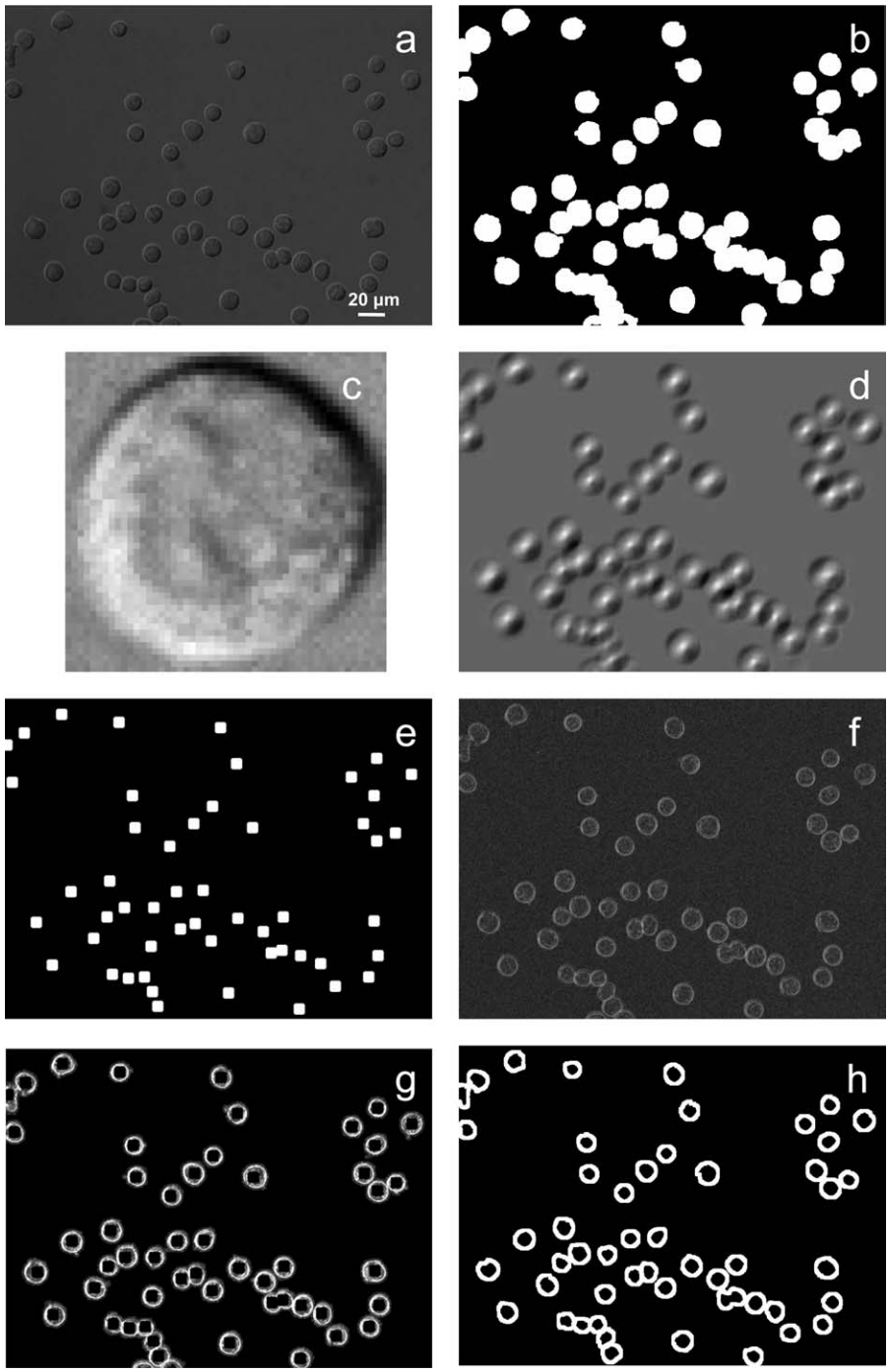

Figure 3. (**a**) DIC image. (**b**) Coarsely-segmented binary image. (**c**) Zoomed in cell template. (**d**) Correlation map (H_k) that is obtained by convolving the cell template (c) and original image (a). (**e**) Cell center map (Z_k) consisting of located cell centers obtained by finding local maxima in H_k and thresholding. (**f**) Gradient of (a). (**g**) Located cell centers in (e) are inverted and imposed as local minima on gradient image (f). (**h**) The boundary of segmented cells outlined by applying watershed to (g).

A high-resolution DIC image and its corresponding coarsely segmented image are depicted in Figures 3a and 3b, respectively. An example cell template is depicted in Figure 3c while the correlation map obtained by applying the cell template to the original DIC image (Fig. 3a) is depicted in Figure 3d. The brightness of pixels in the correlation map show the degree of positive correlation, with the brightest points most likely to be cell centers, so the mostly likely cell centers, depicted in Figure 3e, are generated by thresholding as in Eq. (10). The magnitude of the gradient image M_k is preserved on

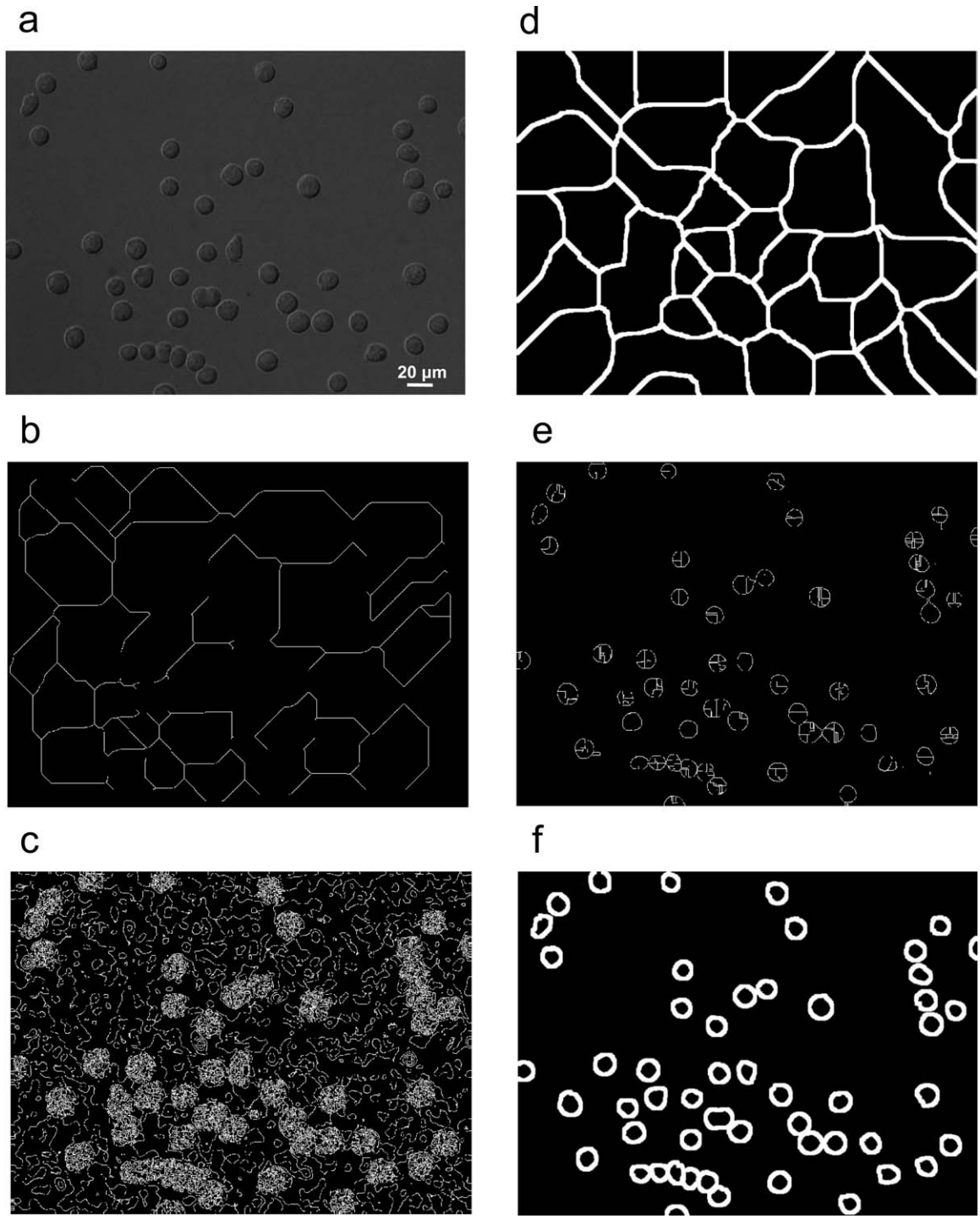

Figure 4. Comparison of conventional watershed and the proposed method. (**a**) Original image. (**b**) Application of watershed to the low pass filtered image. (**c**) Application of watershed to the smoothed magnitude of gradient image. (**d**) Application of watershed to the coarse segmented binary image. (**e**) Application of watershed to the product of binary segmented image and the smoothed magnitude of gradient image. (**f**) The proposed method.

the basis of the corresponding coarsely-segmented binary image O_b, shown in Figure 3b. Then, the detected cell centers (Fig. 3e) are inverted and superimposed on the preserved magnitude image (Fig. 3f) as it is depicted in Figure 3g. At last, the watershed method was used to partition Figure 3g. The resulting segmentation, based on watershed, is depicted in Figure 3h, where the corresponding cell boundaries are outlined. As we can observe, cell boundaries are accurately identified and segmented, both for individual and dividing cells.

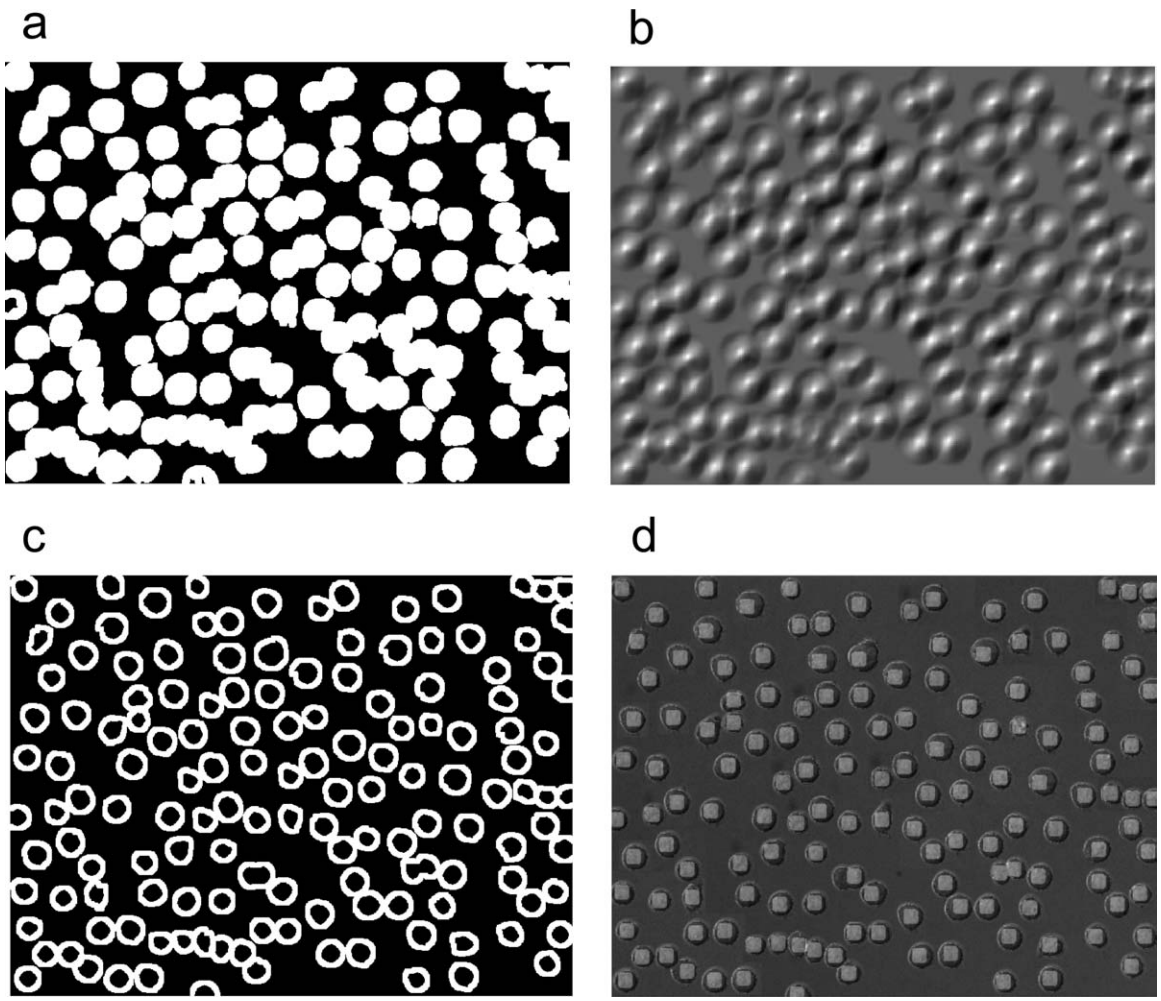

Figure 5. Segmentation of DIC image with crowded cells. (**a**) Coarse binary segmentation. (**b**) Correlation map. (**c**) Outlining the cell boundaries using the proposed method. (**d**) Superimposing the detected centers and outlined boundaries on the original image.

The proposed method is also compared with the conventional watershed segmentation. Figures 4b–4h show the application of watershed to the smoothed original image, to the low pass filtered magnitude of gradient, to the coarse segmented binary image, to the product of coarse binary image and smoothed magnitude of gradient, and to the proposed method, respectively. From the results depicted in Figure 4, it is obvious that the conventional watershed fails to address the DIC cell segmentation problem, while the proposed constrained watershed method not only detects the individual, touching, and dividing cells, but also successfully draws the outline of each cell.

Next, we applied the proposed method to a crowded cell image, synthesized using a few DIC frames. Figure 5a shows the coarse binary segmentation, with the correlation map in Figure 5b. Outlined cell boundaries obtained by the proposed method are shown in Figures 5c and 5d. As can be seen in Figure 5, the performance of the proposed method is significant, successfully detecting and segmenting individual, touching, and dividing cells.

Data sets A, B, C, and D are typical image sequences, each of which consists of 100 image frames with approximately 1,000 cells. Data set E is an image sequence of 200 frames consisting of about 8,500 cells over the entire image set. Figures 6a–6d show the performance of the proposed method for individual cell detection and segmentation.

To quantify the cell detection performance, we counted the number of correctly detected cells in each frame and summed them over each data set, with the detection percentage shown in Figure 6a. To extract the cell centers from the correlation map, the threshold was set to minimize the number of false alarms, implying a false alarm rate of zero. The number of misdetections was counted manually for each data set, with the percentage shown in Figure 6b. Subsequently we manually counted the number of cells that were not segmented and computed the corresponding percentage, shown in Figure 6c; we point out that the unsegmented set is a superset of undetected set, i.e., comprising all undetected cells and those detected cells which were not segmented. At the end for each data set, we visually inspected and marked as bad those

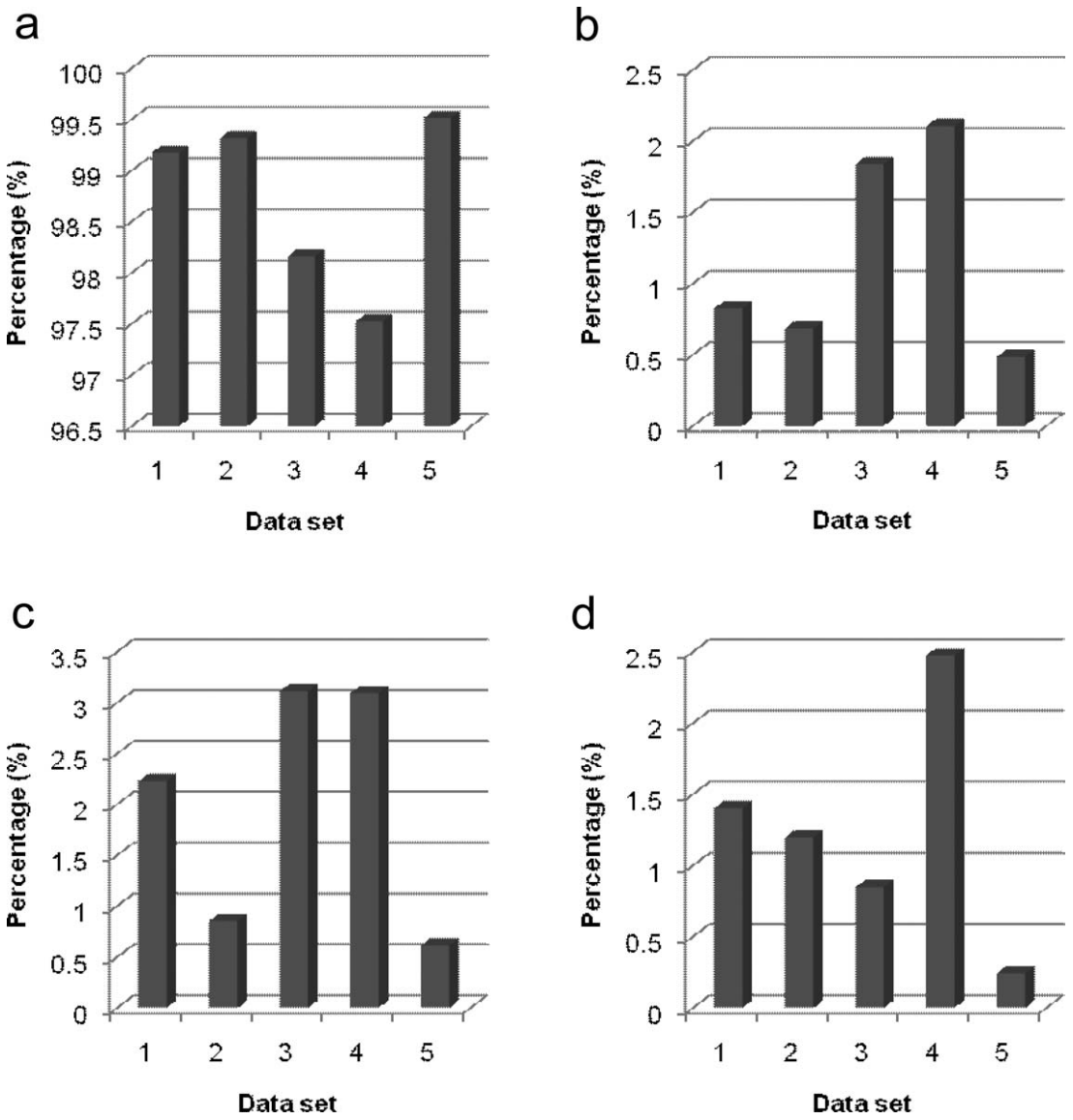

Figure 6. The performance of the proposed method. The detection rate reaches 99.0% while the maximum unsegmented cell ratio is 3.1%, and maximum bad segmentation ratio is less than 2.5%. (**a**) The percentage of detected cells for each data set. (**b**) Undetected cell percentage for each data set. (**c**) Unsegmented cell percentage. (**d**) Bad segmented cell boundaries.

segmented cells for which the outlined boundary was more than 30% over- or under-segmented (Fig. 6d).

As can be observed in Figures 6a–6d, in the worst case (data set D) more than 97.5% of cells are correctly detected (Fig. 6a) while there are fewer than 2.5% undetected cells (Fig. 6b), 3.1% unsegmented cells (which includes undetected cells, Fig. 6c), and 2.5% badly segmented cells (Fig. 6d). The cell detection accuracy reaches 99.5% for data set E, for which 0.5% of cells are undetected, 0.6% unsegmented, and 0.25% badly segmented cells, for 8,500 cells over 200 frames.

There are two types of unsegmentation error in the proposed method:

I. Unsegmented cells with detected cell centers,
II. Unsegmented cells without detected cell centers.

As the centers of some unsegmented cells are indeed localized, and some detected cells are badly segmented, the average cell center detection rate is higher than the cell segmentation rate. The Type I error is improved in comparison with the past work on this problem (22).

The research goal of this article is the large-scale segmentation of cells. That is, although cell segmentation is the image processing part of the article, the use of the segmented cells is the key to the biology side of the research. To this end, segmentation results can be used to potentially extract significant information about cell morphology, area, perimeter, and orientation. Figure 7 shows the histograms of selected features for more than 8,000 cells that were detected and segmented in a DIC image sequence of 200 frames. As can be observed, the cell area, perimeter, orientation, and eccentric-

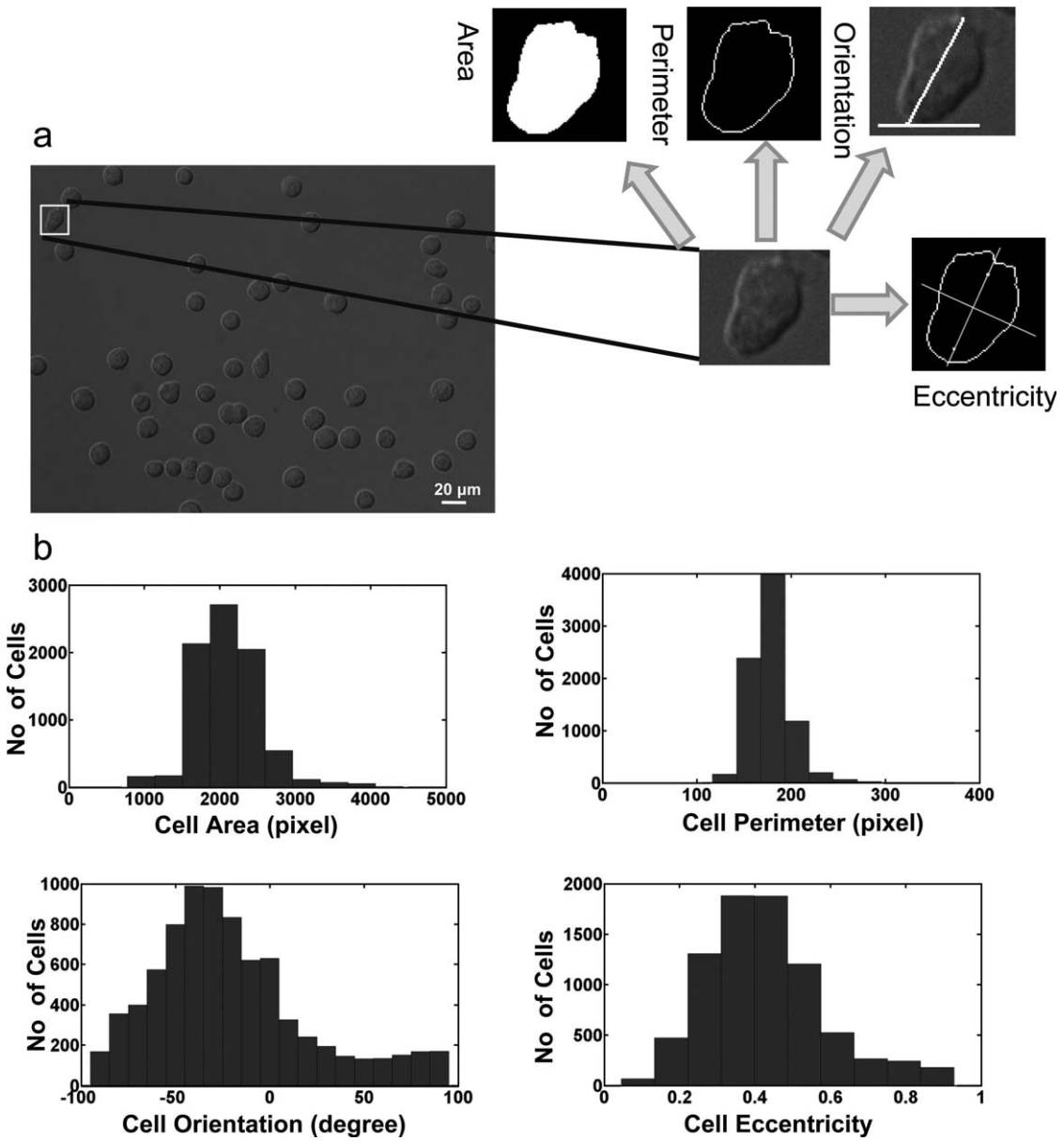

Figure 7. Many different cell features were measured and recorded after applying the proposed method. (**a**) Cell area, perimeter, orientation, and eccentricity of a typical uropodia. (**b**) The distribution (histogram) of cell area, perimeter, orientation, and eccentricity for more than 8,000 cells that were detected and segmented in a DIC image sequence of 200 frames.

ity can all be quantified. We should stress that such information is essential in the study of cell behavior. Our eventual research goal is classifying the presence or absence of cell uropodia for which cell detection and segmentation are the first stage that is completed and presented in this article. To detect such uropods, for example, the cell eccentricity could lead to accurate classification. Our future work is conducted to quantify the accuracy of uropodia classification using the extracted features from the segmented images as the next stage of this project. To achieve this we are in the process of obtaining some sort of ground truth to be used to measure the classification performance.

Figure 8 shows the application of the proposed method to a typical stitched 1,280 × 960 image, a reduced-resolution compilation of nine sub-frames. Detected cell boundaries and cell centers are obtained by applying the proposed method, shown in Figure 8b. As can be seen in the zoomed image of Figure 8c, all cells are detected, whereas two are not segmented. The segmentation performance, correctly locating the cell boundary, of the proposed method for these low-resolution stitched images is over 90%, while the detection performance, locating the cell centers by template matching, is more than 95%. This performance should be improved to the results of the previous images by segmenting the cells in a stitched image

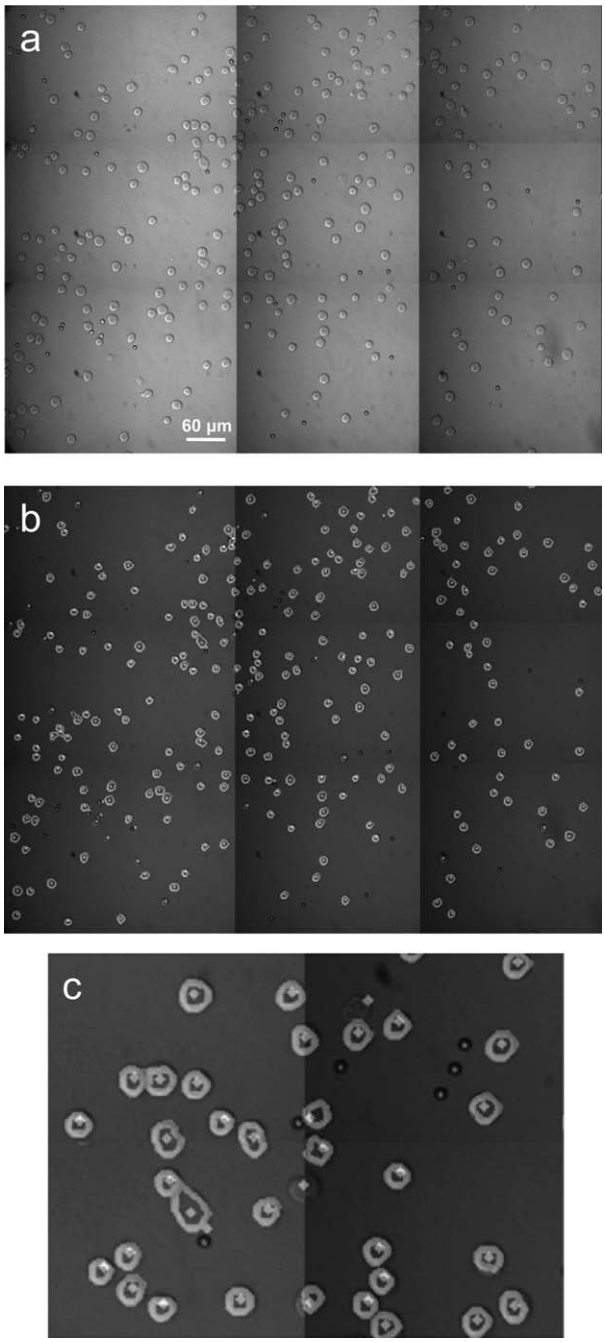

Figure 8. (**a**) A stitched image formed by the stitching of nine subframes. (**b**) The detection and segmentation results obtained by applying the proposed automated segmentation method. Cell boundaries and detected cell centers are marked and superimposed on original image in (a). (**c**) Zoomed in four subframes located in top left of (b).

without down-sampling, albeit at a significant increase in computational time.

A second issue regards the false detection of stationary objects as cell centers. Our experiments were done in a gap chamber where polystyrene beads are used to hold up a layer of glass just over the tops of the cells to reduce turbulence around the bottom of the chamber. As we can observe in Figure 8b, some of the polystyrene beads appear as small black circles with white centers and are detected as cells. These beads are very small in comparison with the cells, and thus the falsely detected centers would not affect the segmentation results; however, these stationary objects can be removed by applying a background estimation method. This may be especially important in such cases where the goal is the tracking of detected cells, and where falsely detected cell centers decrease the performance of tracking.

Conclusions and Discussions

The study of stem cells using digital microscopic image processing is an important application in biomedical research, enabling scientists to measure and extract stem cell properties/features from large volumes of microscopic cell images. Cell segmentation is an essential step in cell analysis, characterization, and tracking. The method proposed in this article is not cell-specific, and can be applied to different cell types.

In the proposed method, cell boundary segmentation is addressed as an inverse problem represented in the form of a constrained problem. In contrast with previous work, in this article the segmentation problem is solved by optimally constructing cell regions associated with cell centers using an optimized watershed method. This is a generic method, capable of segmenting different cell types having arbitrary shapes.

The proposed method is capable of localizing the specific cell types that have been used in our experiments, however to adapt the method for the other cell types that may not have circular shape, the proper cell template must be generated as it is explained in Cell Localization. Further, the proposed method can potentially be used for stem cell research; however it has not been tested for segmenting cells in stem cell aggregates, in particular for circumstances in which neighboring cells significantly overlap with each other, and where cell morphology may considerably change.

The proposed algorithm was applied to bright field cell images, so in situations that cells are fluorescent (for example by adding calceinAM) or where the user needs to distinguish features across cells such as antibody stained cells, the proper cell template(s) must be designed for the fluorescence range of interest. In such cases, if the color stain would spill outside the cell boundary or partially stain the cell area, the cell segmentation might drop in accuracy.

Our future work focuses on methods of background estimation/subtraction, and on greater flexibility in cell template learning using artificial intelligence techniques to extract or generate the proper template from a cell template library.

Literature Cited

1. Kohler A, Schmithorst V, Filippi MD, Ryan MA, Daria D, Gunzer M, Geiger H. Altered cellular dynamics and endosteal location of aged early hematopoietic progenitor cells revealed by time-lapse intravital imaging in long bones. Blood 2009;114:290–298.
2. Kachouie NN, Fieguth P, Ramunas J, Jervis E. Probabilistic model-based cell tracking. Int J Biomed Imag 2006;2006:1–10.
3. Kachouie NN, Fieguth P, Jervis E. Stem-cell localization: a deconvolution problem. Conf Proc IEEE Eng Med Biol Soc 2007;2007:5525–5528.
4. Kachouie NN, Fieguth PW. Extended-Hungarian-JPDA: Exact single-frame stem cell tracking. IEEE Trans Biomed Eng 2007;54:2011–2019.

5. Bowie MB, Kent DG, Dykstra B, McKnight KD, McCaffrey L, Hoodless PA, Eaves CJ. Identification of a new intrinsically timed developmental checkpoint that reprograms key hematopoietic stem cell properties. Proc Natl Acad Sci USA 2007;104:5878–5882.
6. Francis K, Palsson B, Donahue J, Fong S, Carrier E. Murine Sca-1(+)/Lin(-) cells and human KG1a cells exhibit multiple pseudopod morphologies during migration. Exp Hematol 2002;30:460–463.
7. Dykstra B, Ramunas J, Kent D, McCaffrey L, Szumsky E, Kelly L, Farn K, Blaylock A, Eaves C, Jervis E. High-resolution video monitoring of hematopoietic stem cells cultured in single-cell arrays identifies new features of self-renewal. Proc Natl Acad Sci USA 2006;103:8185–8190.
8. Lanzkron SM, Collector MI, Sharkis SJ. Hematopoietic stem cell tracking in vivo: A comparison of short-term and long-term repopulating cells. Blood 1999;93:1916–1921.
9. Giebel B, Corbeil D, Beckmann J, Hohn J, Freund D, Giesen K, Fischer J, Kogler G, Wernet P. Segregation of lipid raft markers including CD133 in polarized human hematopoietic stem and progenitor cells. Blood 2004;104:2332–2338.
10. Comaniciu D, Foran D, Meer P.Shape-based image indexing and retrieval for diagnostic pathology. In: International Conference on Pattern Recognition. Brisbane, Australia: IEEE 1998. pp 902–904.
11. Comaniciu D, Meer P. Cell image segmentation for diagnostic pathology. In: Advanced Algorithmic Approaches to Medical Image Segmentation: State-of-the-art Applications in Cardiology, Neurology, Mammography and Pathology. 2002. pp 541–558.
12. Campo E, Jaffe ES. Mantle cell lymphoma. Accurate diagnosis yields new clinical insights. Arch Pathol Lab Med 1996;120:12–4.
13. Bauman I, Nenninger R, Harms H, Zwierzina H, Wilms K, Feller A, Meulen V, Muller-Hermelink H. Image analysis detects lineage-specific morphologic markers in leukemia blast cells. Am J Clin Pathol 1995;105:23–30.
14. Geusebroek J, Smeulders A, Cornelissen F.Segmentation of cell clusters by nearest neighbour graphs. In: Proceedings of the third annual conference of the Advanced School for Computing and Imaging. 1997. pp 248–252.
15. Meas-Yedid V, Cloppet F, Roumier A, Alcover A, Olivo-Marin JC, Stamon G. Quantitative microscopic image analysis by active contours. In: Vision Interface Annual Conference—Medical Applications. Ottawa: National Research Council of Canada; 2001. pp 277–284.
16. Kittler J, Illingworth J. Minimum error thresholding. Pattern Recogn 1986;19:41–47.
17. Otsu N. A threshold selection method from gray-level histograms. IEEE Trans Syst Man Cybern 1979;9:62–66.
18. Wu K, Gauthier D, Levine MD. Live cell image segmentation. IEEE Trans Biomed Eng 1995;42:1–12.
19. Markiewicz TW, Osowski S, Moszczyski L, Satat R.Myelogenous leukemia cell image preprocessing for feature generation. In: 5th International Workshop on Computational Methods in Electrical Engineering. Warsaw, Poland: Institute of Theory of Electrical Engineering, Measurement and Information Systems, Warsaw University of Technology 2003. pp 70–73.
20. Moogk D, Hanley S, Ramunas J, Blaylock A, Skorepova J, Rosenberg L, Jervis E. Design and analysis of a long-term live-cell imaging chamber for tracking cellular dynamics within cultured human islets of Langerhans. Biotechnol Bioeng 2007;97:1138–1147.
21. Kachouie N, Fieguth P, Ramunas J, Jervis E. A statistical thresholding method for cell tracking. Vancouver, Canada: IEEE International Symposium on Signal Processing and Information Technology. 2006. pp 222–227.
22. Kachouie NN, Fieguth P, Jervis E. Watershed deconvolution for cell segmentation. Conf Proc IEEE Eng Med Biol Soc 2008;2008:375–378.
23. Canny JF. A computational approach to edge detection. IEEE Trans Pattern Anal Mach Intell 1986;8:679–698.
24. Gonzalez RC, Woods RE. Digital Image Processing. New Jersy. Prentice Hall: Prentice Hall; 2002.
25. Beucher S, Meyer F. The morphological approach to segmentation: The watershed transformation. In: Dougherty E, editor. Mathematical Morphology in Image Processing. New York: Marcel Dekker; 1993. Chapter 12.
26. Meyer F, Beucher S. Morphological segmentation. J Vis Comm Image Represent 1990;1:21–45.
27. Beucher S, Lantuejoul C. Use of watersheds in contour detection. Rennes, France: International Workshop on Image Processing, Real-Time Edge and Motion Detection/Estimation 1979. pp 17–21.